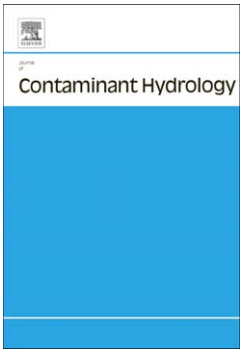

Does phosphate enhance the natural attenuation of crude oil in groundwater under defined redox conditions?

Violaine Ponsin, Olsen Raïnness Mouloubou, Pascale Prudent, Patrick Höhener

PII: S0169-7722(14)00050-3
DOI: doi: 10.1016/j.jconhyd.2014.04.003
Reference: CONHYD 2990

To appear in: *Journal of Contaminant Hydrology*

Received date: 30 October 2013
Revised date: 11 February 2014
Accepted date: 9 April 2014

Please cite this article as: Ponsin, Violaine, Mouloubou, Olsen Raïnness, Prudent, Pascale, Höhener, Patrick, Does phosphate enhance the natural attenuation of crude oil in groundwater under defined redox conditions?, *Journal of Contaminant Hydrology* (2014), doi: 10.1016/j.jconhyd.2014.04.003

Does phosphate enhance the natural attenuation of crude oil in groundwater under defined redox conditions?

Violaine PONSIN[1,2], Olsen Raïnness MOULOUBOU[1], Pascale PRUDENT[1] and Patrick HÖHENER[1*]

[1] Aix-Marseille Université - CNRS, Laboratoire Chimie Environnement FRE 3416, Marseille, France.

[2] French Environment and Energy Management Agency, 20 avenue de Grésillé – BP 90406 Angers Cedex 01, France.

*Corresponding author, phone: ++33 4 13 55 10 34, Fax ++33 4 13 55 10 60, patrick.hohener@univ-amu.fr

Revised Version CONHYD3717

Submission to special issue Groundwater Quality 2013

Abstract

After a crude oil spill caused by a broken pipeline in 2009 to a gravel aquifer in southern France, degradation processes under various redox conditions progressively established, but at rates that predict a long life-time of the source under natural attenuation after partial source removal. In this study, we aimed at identifying the rate-limiting factors for each redox condition, with special emphasis on phosphate as limiting nutrient. The study was conducted in laboratory microcosms assembled with material collected on site: sediments, water from monitoring wells, oil and microbial sludge. Redox conditions were promoted by adding electron acceptors (either oxygen, nitrate, limonite (FeO(OH)), cryptomelane ($K(Mn^{4+},Mn^{2+})_8O_{16}$), or sulfate). For each condition, the role of phosphate was studied by repeated additions for up to 290 days. The results showed a very strong stimulation of aerobic and denitrifying rates of oil degradation by phosphate, provided that oxygen and nitrate were repeatedly supplied. Phosphate caused also a marked stimulation of methanogenic degradation, and a relatively small stimulation of metal reduction. These anaerobic processes started only after marked lag phases, and phosphate shortened the lag phase for methanogenic degradation. Degradation of aromatic and aliphatic hydrocarbons with less than 8 carbons, including benzene, was confirmed even under unstimulated conditions.

It is concluded that degradation rates at the site are limited by both, availability of electron acceptors and availability of phosphate needed for promoting microbial growth.

Key words (max 6)

La Crau nature reserve, Enhancement, Nutrients, Hydrocarbons, Aquifer, Microcosms

1. Introduction

Ground-water contamination by crude oil, and other petroleum-based liquids, is a widespread problem. Although many remediation techniques exist, residual contamination persists after incomplete or inexistent source removal, and natural attenuation occurs. At monitored sites, researchers have gained a good comprehension of processes that control the fate of spilled crude oil. The crude-oil spill site near Bemidji is one of the best characterized sites of its kind in the world (Essaid et al., 2011). At Bemidji, biogeochemical processes have now been studied for more than 30 years, and the following major insights were gained: 1) spontaneous evolution of sequenced redox processes evolves, leading to distinct spatial redox zones; 2) the availability of electron acceptors is a major limiting factor for overall oil degradation; and 3) it takes decades for complete oil removal.

On August 7, 2009 five hectares of land surface and shallow subsurface in a nature reserve of restricted access 50 km northwest of Marseille, south of France, were contaminated by 5,100 m^3 of crude oil (Russian Express) due to the sudden break of a pipeline. Despite immediate cleanup efforts, the most important regional aquifer had been contaminated by gravitational transport of > 200 m^3 of crude oil through the 10 m thick unsaturated zone. Monitored natural attenuation is currently an option for site treatment after completion of physical remediation by dual-phase extraction, but duration of decades is not well accepted. Recently, (Barbieri et al., 2011) have shown how each aquifer redox condition can be induced in laboratory microcosms and how then the factors controlling processes can be studied. Therefore, a microcosm study has been initiated to investigate possibilities of enhancement of natural attenuation under defined redox conditions.

In groundwater, nitrate is usually available as a source of nitrogen (N) whereas phosphorus (P) is often a limiting nutrient. Studies have investigated the stimulation potential of N and P , (Dibble and Bartha, 1979) or the consequences of N-limited environment (Allen-King et al.,

1994)+ (Allen-King et al., 1996) on aerobic petroleum hydrocarbon biodegradation. (Mills and Frankenberger, 1994) evaluated organic and inorganic P sources to promote aerobic bioremediation of diesel fuel. Addition of inorganic P sources can result in precipitation with cations making the P unavailable to the microbes whereas organic P sources need to be mineralized to be available. They showed that diethylphosphate had the higher stimulatory effect compared to potassium phosphate K_2HPO_4. (Bregnard et al., 1996) studied the effect of phosphate on degradation of weathered diesel fuel under aerobic and denitrifying conditions and found that oxygen consumption rates were stimulated by factors of 2-3, and that NO_3^- consumption rate in absence of O_2 was 37 % higher when phosphate was added. To the best of our knowledge, no studies investigated whether P can stimulate rates of anaerobic petroleum hydrocarbons biodegradation under other redox conditions.

Several studies conducted at Bemidji revealed that phosphate- and iron-bearing minerals were attacked by microorganisms. (Hiebert and Bennett, 1992) performed an in situ microcosm study of the influence of surface-adhering bacteria on quartz and feldspar diagenesis. They showed that minerals were colonized by indigenous bacteria and chemically weathered at a rate faster than theoretically predicted. Another in situ microcosm study revealed that native organisms preferentially colonized feldspars that contain trace P as apatite inclusions (Bennett et al., 2000). These feldspars weathered rapidly, whereas nearby feldspars without trace P were uncolonized and unweathered. (Rogers and Bennett, 2004) addressed the question of whether the microbial community benefits from release of minerals during weathering. Their study showed that in microcosms containing silicates and glasses with trace phosphate mineral inclusions microbial biomass increased, indicating that the microbial community can use silicate-bound phosphate inclusions. They proposed that microorganisms may use organic ligands to dissolve the silicate matrix and access these otherwise limiting nutrients. (Bekins et al., 2005) studied local differences in n-alkane degradation and found that recharge-facilitated

transport of phosphate and nitrate were the most-likely factors for explaining variances in degradation rates.

Like P, bioavailable Fe and Mn can be scarce in groundwater because of the low solubility of iron and manganese oxyhydroxydes at neutral pH. At Bemidji temporal changes related to limited availability of iron and manganese have been observed (Baedecker et al., 1993), (Cozzarelli et al., 2001). Mn^{2+} increased, peaking 8 years after the spill, and then decreased, suggesting that the manganese available for reduction was being depleted. Fe^{2+} concentration began to increase following the drop in Mn^{2+} and peaked 11 years after the spill (Essaid et al., 1995). (Tuccillo et al., 1999) did a quantitative examination of the Fe geochemistry in Bemidji using several extraction techniques on sediments (Heron et al., 1994), (Ryan and Gschwend, 1991). They showed that prolonged Fe(III) reduction had caused measurable changes in the sediment Fe geochemistry.

In order to understand the limiting factors for crude oil degradation at the La Crau site, the objectives of this study were (1) to simulate each redox condition observable on site and to study its limitation by electron acceptor availability, (2) to assess whether phosphate could shorten the lag phase of processes which appeared slowly at the field site (iron-reduction or methanogenesis) and (3) to study the impact of phosphate on degradation rates and types of kinetics of electron acceptor consumption.

2. Material and Methods

2.1. Site description

The site is in the “La Crau” alluvial plain formed by the former river Durance (Naudet et al., 2004). These deposits are made of coarse gravel with fine gravel and sand in the interstices, cemented near the surface in the form of Puddingstone with fractures. These layers overlay silt or sandy-silt deposits of low permeability (unpublished classified report). The “La Crau”

reserve is a steppe grazed by low numbers of sheep, and the underlying aquifer shows low concentrations of nitrates (5-10 mg/L) and phosphate (< 0.2 mg/L).

The remediation of the surface soils by replacement and off-site disposal of contaminated top soils has been completed. The remediation of aquifer contamination is still ongoing in 2013 and consists in plume management by hydraulic groundwater barriers with re-injection of activated charcoal-treated waters, and dual-phase oil extraction in the source zone. So far, the oil extraction permitted the recovery of 31 m^3 of oil in 3.5 years.

Several wells in the plume were sampled in April 2010 in order to investigate redox conditions nearly one year after the spill. This field study showed that a wide range of redox processes from aerobic respiration to sulfate reduction was observable in the plume. Microbiological investigations suggested that the majority of cultivable microorganisms were sulfate-reducing strains (unpublished classified report). Methane has been detected 2 years after the spill and dissolved CH_4 concentrations doubled every six months since then.

2.2. Water, sediments and crude oil sampled on site

Uncontaminated sediments were collected from 8-9 m depth in a quarry located a few hundred meters away from the spill site at La Crau. The coarse fraction > 4 mm and the fine fraction < 0.124 mm were removed by wet sieving. Sediments were treated repeatedly with H_2O_2 (30%) to remove organic matter.

Water used in experiments was collected from 2 different monitoring wells on site. Pz 39 is upstream of the source where water contained dissolved oxygen up to 8 mg/L, 5 mg/L nitrate and 60 mg/L sulfate. Pz 23 is in the source zone where water was free of oxidants. Both wells were purged prior to sampling, and samples were stored at 4°C before microcosm assembling. Oil was collected on site in an oil-water separator which receives oil from the dual-phase extraction in the source zone. A sludge formed by indigenous microorganisms was also collected in this separator. Oil and sludge were both stored at 4°C after sampling.

2.3. Preparation of solutions and minerals

Solutions of respectively 15 g/L of nitrate ($NaNO_3$), 15 g/L of sulfate (Na_2SO_4), 1 g/L of phosphate (Na_2HPO_4, 12 H_2O) were prepared to supply electron acceptors and P. To inhibit microbial growth, a solution of 25 g/L of sodium azide (NaN_3) was prepared.

An iron mineral, limonite (FeO(OH)), and a manganese mineral, cryptomelane ($K(Mn^{4+},Mn^{2+})_8O_{16}$; (Beauvais et al., 1987), were used to supply iron or manganese and to promote the metal-reducing conditions in some microcosms (both provided by the Laboratoire de Geologie Structurale et Appliquee from Aix Marseille University). Both minerals were separately crushed into particles with a diameter of less than 2 mm before use.

2.4. Assembling and storage of microcosms

We prepared microcosms in 121 mL glass vials (Supelco) that were sealed with Teflon Mininert valves (Supelco). Ten grams of sediments and groundwater in volumes given in Table 1 were filled in each bottle. 250 mg of crude oil and 100 µL of microbial sludge were added before sealing the bottles. Two series of microcosms were prepared: series 1 for frequent gas and water sampling, and series 2 for (destructive) sampling of oil. All microcosms were assembled according to Table 1. Headspace was flushed with N_2 in anaerobic microcosms (Table 1). Bottles and sediments used to assemble the sterile controls (STE) were heated at 110°C for an hour and water was boiled before assembling. 250 mg/L of sodium azide was added to microcosms before sealing. Another set of control microcosms did neither receive oil nor sludge (OIL-). No particular redox condition was promoted in the NAT set in order to monitor the evolution of the electron acceptors consumption starting from oxygen. For each redox condition 3 replicates were amended with 10 mg/L of phosphate (P added at the end of set name) and 3 were not. The STE, NAT and OIL- sets were made of only 3 replicates that did not receive phosphate. Series 1 included 45 microcosms which were

stored under water in the dark at in situ temperature of 18°C and removed regularly for sampling.

When phosphate or an electron acceptor had been entirely consumed in a set of microcosms more solution was added from a solution which was flushed with N_2 before injection. When oxygen was consumed in OXY(P) microcosms they were opened to allow renewal of headspace.

Another group of microcosms (series 2) was prepared identically to series 1 according to Table 1, with 3 sterile replicates and 9 microcosms for each redox condition. None of the sets received phosphate. The 66 microcosms prepared were stored under water in the dark at in situ temperature of 18°C. 3 replicates by set were sacrificed at 3 different times during experiment in order to monitor BTEX and alkane depletion.

2.5. Water and gas sampling during microcosms study

Before water sampling, a volume of N_2 equal to the water volume to be withdrawn was added with a syringe equipped with a needle thin enough to go through the Mininert valve. Water withdrawn by the syringe was filtered through 0.45 µm PTFE filters and kept at 4°C before analysis in the following days. Samples intended for atomic absorption spectrometry (AAS) were immediately acidified (1% hydrochloric acid Ultrapure TraceMetal Grade 34-37 %, Fisher Scientific). Headspace gas was sampled with a gas-tight syringe (Hamilton, Switzerland) equipped with a Teflon plunger. 100 µL or 500 µL of headspace were sampled and directly injected for analysis.

2.6. Water and gas analyses

Anions (F^-, Cl^-, NO_3^-, NO_2^-, SO_4^{2-}, PO_4^{3-}) and major cations (K^+, Na^+, Ca^{2+}, Mg^{2+}) were analyzed by high performance ion chromatography (HPIC) using a Dionex ICS-3000 instrument. Total soluble iron and manganese were analyzed by AAS using a Thermo Scientific ICE 3000 Series instrument. Alkalinity was measured by titration using a Thermo

Scientific Orion 2 Star pH meter using the Gran plot method (Gran, 1950). Dissolved Inorganic Carbon (DIC) was calculated from alkalinity and pCO_2.

Oxygen and carbon dioxide in headspace gas were monitored by gas chromatography with thermal conductivity detector (GC-TCD) using a Shimadzu GC-81 instrument. Samples of 100 µL (oxygen analysis) or 500 µL (carbon dioxide analysis) from the headspace of microcosms were manually injected in splitless injection. Methane in headspace was analyzed by gas chromatography with flame ionization detector (GC-FID) using a Varian 3800. Samples of 100 µL gas from the headspace were manually injected. BTEX and alkanes in series 2 were analyzed by GC-FID using a Perkin Elmer Clarus 580. Sampling was made with a TurboMatrix headspace sampler HS-40 (Perkin Elmer Inc., USA). Details about the different analyses are given in Supp. Material.

2.7. Sediment analyses

Extractions were performed on original sediments, limonite and cryptomelane and on weathered sediments from NAT, FER(P) and MAN(P) in order to complete mass balances. The 0.5 M HCl extraction was used as an assay for microbially reducible Fe(III) and was expected to remove Fe(II) and Fe(III) from amorphous and poorly crystalline Fe phases (Tuccillo et al., 1999). Speciation of Fe(II) and Fe(III) was determined using the Ferrozine method that gives Fe(II) and Fe total (Viollier et al., 2000). Sediments were dried in a glove box filled with N_2. 1 g of sediments and 30 mL of 0.5 M HCl were filled in PTFE centrifuge tubes that were crimped and placed on a shaker table for 5 days. Tubes were centrifuged at 11,000 rpm for 10 minutes and supernatant was filtered through 0.45 µm PTFE filters and stored for analysis.

The Ti-citrate-EDTA-bicarbonate extraction was expected to reductively dissolve amorphous and crystalline Fe(III) oxides. The extraction was performed as described in (Ryan and Gschwend, 1991). Extraction time was extended to 24 hr (Tuccillo et al., 1999). Sample sizes

ranged from 0.01 to 0.5 g. Upon removal from the shaker table, samples were centrifuged at 11,000 rpm for 10 minutes and supernatant was filtered through 0.45 µm PTFE filters and stored for analysis.

Mineralization was expected to provide pseudo-total Fe, Mn and P. 0.5 g of samples were mineralized in a microwave mineralizer (Milestone Start D) using *aqua regia* (1/3 HNO_3 + 2/3 HCl). Concentrations for each extraction were determined by ICP-AES (Jobin Yvon Horiba, Spectra 2000) for total Fe, Mn and P. Limits of quantification were of 3.4, 0.6 and 55 µg/L for Fe, Mn and P respectively.

2.8. PHREEQC simulations

Saturation index for minerals were modeled by using concentrations of dissolved analytes, measured partial pressure of gases and the PHREEQC geochemical model, vs. 2.18 with phreeqc.dat and minteqv4.dat databases for comparison, except for hydroxyapatite (phreeqc.dat and llnl.dat, (Parkhurst and Appelo, 1999).

3. Results

3.1. Control experiments

The control experiments included three sets of microcosms which were heated and poisoned by NaN_3 (set STE), or received neither oil nor sludge (set OIL-), or were run under non-promoted conditions (set NAT). The results from these 3 sets of microcosms are shown in Figure 1 and Figure 2. After an initial drop, the oxygen concentration remained constant at about 10 % in STE microcosms from day 56 until day 288 while carbon dioxide rose to about 2.5 % (Fig. 1. A). There was a small increase in nitrate and no significant evolution in HCO_3^- concentrations in OIL- microcosms after 225 days of monitoring (Fig. 1. B). Oxygen and nitrate were completely depleted after 20 days in NAT microcosms (Fig. 2. A). Then sulfate was consumed between day 50 and day 170 and methanogenesis started after 200 days of

monitoring (Fig. 2. A). HCO_3^- concentration increased in NAT microcosms to reach a plateau during methanogenesis (Fig. 2. B).

3.2. Aerobic and denitrifying microcosms

Aerobic respiration was tentatively stimulated by using repeated air injection to microcosm headspace and denitrification was promoted by enhanced nitrate concentration in denitrifying microcosms. The results from these sets of microcosms are shown in Figure 3. There was a noticeable difference between microcosms amended with phosphate and P-unamended microcosms in both experiments. Oxygen was consumed in approximately 14 days in OXYP microcosms whereas there was still 3 % of oxygen remaining after 122 days of monitoring in OXY microcosms (Fig. 3. A). Nitrate was consumed in 35 days and then 42 days in NITP microcosms whereas its complete consumption lasted 140 days in NIT microcosms (Fig. 3. B). P-amended aerobic microcosms showed also a noteworthy difference to unamended ones in carbon dioxide production (Fig. 3. E). A significant higher HCO_3^- increase was observed in the NITP set compared to NIT (Fig. 3. D). In contrast, there was no such difference regarding HCO_3^- concentrations for OXY and OXYP sets (Fig. 3. C) and carbon dioxide content for NIT and NITP sets (Fig. 3. F).

3.3. Manganese-reducing and iron-reducing microcosms

The results from the sets of microcosms where manganese and iron minerals were supposed to promote the respective conditions are shown in Figure 4. Dissolved manganese concentrations reached values of up to 15 mg/L and 29 mg/L in MAN and MANP microcosms respectively (Fig. 4. A). FER(P) sets did not show such a difference between microcosms amended with phosphate and microcosms not amended. Concentrations in total dissolved iron remained lower than 6 mg/L in both sets (Fig. 4. B). Both concentrations in dissolved manganese and HCO_3^- tended to stabilize or decrease after 70 days in MAN and MANP sets (Fig. 4. A and C), while carbon dioxide values remained low in both sets (Fig. 4.

E). Inorganic carbon showed net increases in both FER and FERP sets with slightly higher concentrations of HCO_3^- in FERP microcosms (Fig. 4. D and F).

3.4. Sulfate-reducing and methanogenic microcosms

Sulfate-reducing conditions were assayed by adding a solution of sulfate to microcosms and methanogenesis was promoted by using water depleted in electron acceptors to assemble microcosms. The results from these microcosms are shown in Figure 5. A lag phase of respectively 83 and 62 days preceded the consumption of sulfate and a substantial production of HCO_3^- in both SUL and SULP sets (Fig. 5. A and C). Thereafter, sulfate was consumed, and the color of the sediment turned from grey to black, suggesting precipitation of metal sulfides. Methanogenesis started after 78 days in METP and 135 days in MET with concentrations about 5 times higher in METP than in MET (Fig. 5. B). Concentrations in HCO_3^- remained constant in MET and METP microcosms (Fig. 5. D). Carbon dioxide in headspace increased without lag phase in both SUL(P) and MET(P) experiments, similarly as in the sterile controls (Fig. 5. E and F).

3.5. BTEX and alkanes in series 2

BTEX and alkanes depletion was monitored through sacrifices of microcosms from series 2. Results for BTEX are summarized in Table 2. Benzene disappeared in every set of microcosms except in poisoned controls. However, > 90 % depletion was achieved only in OXY, NIT, FER and SUL sets at the end of the monitoring. Ethylbenzene and xylenes were depleted > 90 % in every set except for MET and poisoned controls. A small percentage of *o*-xylene was also persistent in NIT microcosms. *1,2,4*-trimethylbenzene (TMB) was depleted > 90 % only in OXY and NIT. Surprisingly toluene was depleted > 90 % at the end of the monitoring only in OXY, SUL and MET, whereas its concentration increased to values above initial concentrations in NAT and FER sets. During monitoring, MAN and MET microcosms also showed an increase in toluene concentration before it dropped until zero for MET (data

not shown). NIT showed a complete depletion of toluene before its reappearance (data not shown). Benzene was degraded faster than toluene in SUL set. Analyses in GC-MS confirmed results obtained in GC-FID and permitted to quantify benzene which was co-eluted with cyclohexane in GC-FID

Gas chromatograms presented in Figure 6 show volatile hydrocarbons from 4 to 12 carbon atoms in a STE microcosm (Fig. 6.A), in a NIT microcosm after 199 days of incubation (Fig. 6.B) and a MET microcosm after 312 days of incubation (Fig. 6.C). NIT and MET chromatograms were depleted in light molecules compared to STE and showed other compounds with peak heights at lower signals. The analysis revealed that *n*-pentane, *n*-hexane, (*m,p*)-xylenes and *1,2,4*-TMB were completely degraded in NIT microcosm. There were only traces left of benzene + cyclohexane, *n*-heptane, *n*-octane, ethylbenzene, *n*-nonane and *n*-decane. MET microcosm showed a complete degradation of pentane whereas *n*-hexane, benzene + cyclohexane, *n*-heptane, toluene, ethylbenzene, xylenes, *n*-nonane and *n*-decane were partially degraded.

4. Discussion

4.1. Promotion of redox conditions

In unstimulated microcosms with oil (NAT set), a succession of redox conditions could be observed which followed what is expected from thermodynamic theory: an initial rapid oxygen reduction was accompanied by rapid and complete nitrate reduction (Fig. 2. A). Then, metal-reducing conditions may have prevailed for about 30 days, but the availability of manganese and iron was not sufficient to prevent sulfate from decreasing after 50 days. Methanogenic conditions with CH_4 production were established only after complete disappearance of sulfate after 160 days. The abiotic (poisoned and heated) controls as well as the controls without oil showed insignificant increases in inorganic carbon. Electron acceptors were not depleted, and even increased slightly in case of nitrate in OIL- set due to

nitrification. Natural organic matter can be excluded as electron donor in this experimental set-up.

Specific redox conditions were successfully achieved and maintained for up to 10 months in all oil-containing sets which initially were aimed at being stabilized in specific redox states. Since oxygen and nitrate consumption were fast, these oxidants had to be added in the course of the experiment.

Oxygen consumption in OXY microcosms was surprisingly slow (Fig. 3. A), especially compared to oxygen consumption in NAT (Fig. 2. A), which was four times faster for the same initial content. Despite this result OXY set is the only set that showed a complete depletion for each BTEX quantified (including *1,2,4*-TMB) at the end of the monitoring (Table 2).

In NIT and NITP sets, nitrite appeared transiently during monitoring (Supp. Material, Fig. S1). Nitrite remained lower than 30 mg/L in NITP whereas concentrations reached 60 mg/L in NIT microcosms. In both sets nitrite was consumed only after depletion of nitrate. An explanation for this accumulation of nitrite may be that nitrite reductase is repressed at high pH conditions due to both scarcity of electrons and competition with nitrate reductase for the flow of electrons (Almeida et al., 1995), (Glass and Silverstein, 1998). This repression ends when there is no more nitrate available or when pH drops.

In FER(P) microcosms, dissolved iron concentrations remained low during monitoring. In MAN(P) sets manganese concentrations reached a maximum and then decreased probably because of precipitation (see 4.4.). Sulfate-reduction was observable after about 70 days in FER(P) and MAN(P) sets (data not shown), whereas dissolved Mn concentrations were still increasing in MAN(P). The slow dissolution of the sediments was likely a rate limiting factor for iron and manganese reductions, and sulfate-reduction probably occurred simultaneously after 70 days. Concomitant iron and sulfate-reductions have already been observed in field

and laboratory studies (Brown et al., 2000) (Chapelle et al., 2009), (Jakobsen and Postma, 1999), (Barbieri et al., 2011). Strictly manganese- or iron-reducing conditions cannot be maintained for a long time in laboratory experiments in the presence of sulfate when natural Fe and Mn sources are used.

Chemical extractions were performed on initial sediments, limonite and cryptomelane, to evaluate available Fe, Mn and P for microorganisms. Initial addition of limonite in FER and FERP sets only slightly increased the quantity of microbially reducible Fe(III) (Table 3). Addition of cryptomelane in MAN(P) sets increased the quantity of available Fe(III) by 50 % and the quantity of Mn extractable with 0.5 M HCl by 300 %. These results suggest that cryptomelane contained both crystallized iron and manganese minerals, but less iron than limonite, and that not only manganese was supplied to MAN(P) but also iron, and traces of P. The time scales for the establishment of sulfate-reducing and methanogenic conditions were similar to those in the NAT set. The sludge collected in the separator had been in contact with oxygen on site and during storage. SUL and NAT sets showed a lag phase before sulfate-reduction of 83 days and 50 days respectively, whereas MET and NAT sets showed a lag phase before methanogenesis of 135 days and 200 days respectively (Table 4). The slightly longer lag phase prior to methanogenesis in NAT was due to the presence of other oxidants such as oxygen and nitrate at the beginning of the monitoring. Likewise, the availability of manganese and iron-oxides may have contributed to retarded establishment. In an approach similar to ours, (Townsend et al., 2003) observed the same lag phase of 50 days before the beginning of observable sulfate-reduction and an even shorter lag period (60-80 days) before significant methane production in aquifer slurries. Methane was detected on La Crau site for the first time only 27 months after the spill. Microcosms are closed systems while at the field site there is a constant renewal of electron acceptors, especially with the ongoing physical remediation. Maximum methane concentrations in microcosms remained lower than 0.5 mg/L

(MET set) whereas they reached values up to 6.7 mg/L on site where they approximately double every six months. In MET(P) sets there was little electron acceptor available (sulfate < 5 mg/L) apart from iron and manganese in sediments, explaining a shorter lag period than NAT. The lag period for SUL(P) and MET(P) sets may also be related to a phase of growth of sulfato-reducing and methanogenic microorganisms.

4.2. P as limiting factor?

The sediment from the Crau aquifer had a HCl-extractible P content of 0.11 mg g^{-1} (Tab. 3). This is rather at the low end of P contents reported from minerals found at the Bemidji site (<0.05 in quartz or calcite to 3 mg g^{-1} in basalt, Bennett et al, 2000). In microcosms, phosphate showed a stimulating effect on methane production (methanogenic sets), inorganic carbon production (iron-reducing sets) or both electron acceptor consumption and inorganic carbon production (OXY(P), NIT(P), MAN(P) and SUL(P) sets). Successive addition of oxygen or nitrate in OXYP and NITP sets respectively showed that the limiting factor for natural attenuation is the availability of electron acceptors and not the availability of hydrocarbons. In sulfate-reducing sets, the lag phase was shortened by 21 days in P-amended microcosms compared to unamended ones (Table 4). In methanogenic sets, the lag phase was shortened by 57 days and production of methane was between 4 and 10 times higher in METP microcosms.

Phosphate completely or partially disappeared in each amended set and was therefore added in OXYP, FERP, MANP and METP sets (Fig 7.). NITP set showed little depletion of phosphate despite a strong stimulating effect compared to NIT microcosms (Fig. 3. B.). In contrast FERP and MANP displayed the highest depletion. Addition of inorganic P sources can result in precipitation with iron, manganese and calcium (Mills and Frankenberger, 1994). PHREEQC simulations showed that vivianite ($Fe_3(PO_4)_2$:$8H_2O$) was undersaturated whereas hydroxyapatite ($Ca_5(PO_4)_3OH$) was over-saturated in P-amended microcosms at the beginning

of the monitoring (Supp. Material, Fig. S2). At intermediate times saturation indexes were comprised between 0.9 and 2.3 for vivianite, 0.9 and 3.7 for hydroxyapatite. Despite over-saturation there was still phosphate in solution, sometimes several weeks after the initial addition (Fig. 7). (Pan and Darvell, 2010) showed that the solubility of pure hydroxyapatite increased with an increase in pCO_2 when studying the effect of carbonate on solubility of calcified tissues in vertebrates. Ito et al. (1997) revealed that the equilibrium solubility of OH-carbonated hydroxyapatite ($Ca_{10}(PO_4)_6(CO_3)_x(OH)_{2-2x}$) increased with an increase of carbonate content. The geochemical databases in PHREEQC do not include carbonated hydroxyapatite and therefore largely underestimate the solubility of hydroxyapatite.

There was only a little depletion of dissolved phosphate in sulfate-reducing microcosms (Fig. 7. E). Sulfate depletion in SUL and SULP started after respectively 83 and 62 days of monitoring (Table 4). Ammonium was added to both sets after 115 days of monitoring and sulfate-reduction increased after this addition. This suggests that N may also be a limiting nutrient for sulfate reduction. Indeed, the water used to assemble SUL and SULP sets was completely depleted in nitrate.

Extractions were made on sediments from NAT, MAN(P) and FER(P) sets after disassembling the microcosms. Slightly more Fe(II) was extractable with 0.5 M HCl in the final FERP set than in FER set. These results suggest that iron-bearing minerals may have been more attacked in P-amended microcosms resulting in more intense precipitation of ferrous-iron minerals (see 4.4.). This is consistent with a slightly higher production of HCO_3^- (Fig. 4. D).

4.3. Degradation of hydrocarbons

Analyses made right after the spill revealed that Russian Express contained 0.09 % (w/w) of benzene and 0.17 % of toluene (unpublished classified report). However, the oil sampled on site 2.5 years after the spill which was used for microcosm assembling was already strongly

depleted in toluene compared to benzene. Therefore, initial toluene concentrations in the microcosms were close to our detection limit.

A marked disappearance of benzene, ethylbenzene and xylenes was noted under all promoted redox conditions, whereas for toluene, final concentrations were sometimes higher than initial concentrations, but remained near our detection limit.

While the mechanisms for anaerobic metabolism of toluene, ethylbenzene and xylenes are fairly well known (Weelink et al., 2010), the mechanism for benzene degradation remains unknown despite numerous studies trying to elucidate it. Three pathways have been proposed: methylation to toluene, hydroxylation and carboxylation (Coates et al., 2002), (Chakraborty and Coates, 2005), (Meckenstock and Mouttaki, 2011), (Vogt et al., 2011). (Ulrich et al., 2005) provided the first and so far only direct evidence to support the methylation pathway by adding $^{13}C_6$-benzene to nitrate-reducing and methanogenic enrichment cultures. In both cultures [ring-^{13}C]-toluene was detected transiently during degradation. Their data strongly support initial methylation of benzene to toluene, followed by transformation to benzoate. Detection of phenol in methanogenic culture suggested that two parallel pathways may be operative in this condition. Our results suggest that toluene could be an intermediate for benzene anaerobic degradation also in iron, manganese or sulfate-reduction. To the best of our knowledge there is no study showing that toluene could be an intermediate for benzene anaerobic degradation under these redox conditions.

Comparison of GC-MS analyses showed that *1,2,4*-TMB was the most depleted trimethylbenzene isomer followed by *1,3,5*-TMB. *1,2,3*-TMB was recalcitrant to degradation in all sets (results not shown). This observation is consistent with a previous study under denitrifying conditions (Häner et al., 1997). Figures. 6.B. and C. show further persistent unidentified peaks at 14.6 minutes of retention time for MET microcosm, 22.6 minutes for NIT and MET, and 24 minutes for NIT. Analyses in GC-MS did not allow identification, but

comparison between Figure 6. B. and chromatograms from (Häner et al., 1997) suggests that the peak at 22.6 minutes could be 2-ethyltoluene, which was not metabolized in their study.

4.4. Degradation rates, inorganic carbon production and kinetics

In order to better compare the effectiveness of each electron acceptor, degradation rates of electron acceptors and carbon production for each set of microcosms will be calculated here. Electron acceptor consumption rates in mmoles electrons per liter per day for each series (average on whole period) are displayed in Figure 8. A. Only OXYP and NITP sets had higher rates than NAT set (about 24 times higher for OXYP microcosms).. Mineralization on initial minerals in FER(P) sets showed that they contained 68 mg total Fe/g mineral. Only 1 mg was Fe extractible by 0.5 M HCl: 2/3 Fe(III) and 1/3 Fe(II) (Supp. Material, Fig. S3). Final extractions showed an increase in Fe(II) content in both sets whereas HCL-extractible Fe(III) content was slightly lower in FER microcosms and slightly higher in FERP microcosms. This last observation could tentatively be explained by greater silicate weathering in FERP. Consumption rates for FER(P) sets were completed with results from extractions (Fig. 8. A).

Inorganic carbon in mmoles of carbon produced for each series may therefore be a better tool for process comparison. They are displayed in Figure 8. B. OXYP and NITP had higher total inorganic carbon productions compared to the NAT set (about 2 times higher for OXYP microcosms) whereas the OXY and NIT without P produced inorganic C about equally. Inorganic carbon production was about equal under iron-reducing and sulfate reducing conditions. Under manganese-reducing conditions, the carbon production was either very small (with P), or a net carbon consumption was observed (without P), probably as a result of precipitation of a carbonate mineral. Due to such precipitations, the inorganic carbon production in Figure 8. B must be interpreted with caution.

After renewals of headspace in OXYP microcosms, the carbon dioxide always remained higher than atmospheric partial pressure (Fig. 3. E). At the same time HCO_3^- concentrations slightly decreased after some renewals (Fig. 3. C). Decreases in carbon dioxide content in headspace were probably responsible for a shift in balance given in Eq. 1.:

$$CO_2 + H_2O \Leftrightarrow H_2CO_3 \Leftrightarrow H^+ + HCO_3^- \quad (1)$$

Furthermore, temporal fluctuations in HCO_3^- were also observed in microcosms without oil. Moreover, the complex composition of crude oil makes precise determination of the expected stoechiometry of terminal electron accepting processes difficult, so we did not try to weigh electron acceptors consumption against inorganic carbon production.

The geochemistry of some sets at the beginning and the end of the monitoring was simulated with PHREEQC. Simulations showed that calcite tended to become undersaturated with time and was dissolved (Fig. 9. A.), whereas siderite (Fig.9. B.) and rhodochrosite (Fig. 9. C.) tended to become over-saturated and precipitated. These results suggest that dissolved inorganic carbon contents in microcosms were controlled by calcite, siderite, and rhodochrosite. Low concentrations of Fe, Mn and HCO_3^- observed in FER(P) and MAN(P) sets can be linked to precipitations of dissolved ferrous iron and manganese with carbonate. These assumptions were confirmed by extractions made on final sediments that showed that more Fe(II) was extractable with 0.5 M HCl in final NAT and FER(P) sets compared to initial composition (Supp. Material, Fig. S3)

Types of electron acceptor consumption kinetics are shown in Table 4. The only sets with first-order kinetics were OXY(P) sets while other sets displayed Monod-with-growth kinetics. The difference of kinetics may be explained by the fact that oxygen is in the gaseous phase whereas other electron acceptors are dissolved or solids. Modeling of natural conditions should include Monod kinetics rather than first-order kinetics.

5. Conclusions

The strongest stimulating effect of phosphate has been observed in oxygen and nitrate-amended microcosms. If in situ stimulation of biodegradation through addition of nitrate or oxygen (e.g. biosparging) was implemented at the La Crau site, phosphate should be added to improve the rate of oil degradation.

Another significant effect of P was that it shortened the lag phase in methanogenic microcosms and increased the production of methane. At the field site, P injection throughout the source zone without electron acceptor addition will most likely lead to a broader core zone with stimulated methanogenesis and narrower redox fringes at the source margins. In P-amended sulfate-reducing microcosms, P shortened the lag phase only slightly. Phosphate had a stimulating effect on iron-reduction but added minerals had low iron bioavailability. Kinetics of iron-reduction remained low in both P-amended and unamended microcosms. Phosphate was maintained in aqueous solution during weeks despite oversaturation with respect to hydroxyapatite, but tended to precipitate as iron- and manganese minerals under metal-reducing conditions. Further studies need to be done on iron phases existing in La Crau site to assess whether iron can be a main electron acceptor for natural attenuation.

We successfully observed degradation of recalcitrant compounds such as benzene or *1,2,4*-TMB under various redox conditions including methanogenesis. These processes have been seen even without addition of phosphate. More work needs to be done regarding the possible production of trace amounts of toluene during benzene degradation under a wider range of redox conditions.

Acknowledgements

The authors gratefully acknowledge financial support by ICF Environnement, Société du Pipeline Sud-Européen, ADEME and the CNRS Federation ECCOREV (Ecosystèmes Continentaux et Risques Environnementaux). We thank Carine Demelas and Laurent Vassalo for their technical assistance and Anicet Beauvais for providing cryptomelane.

References

Allen-King, R.M., Barker, J.F., Gillham, R.W. and Jensen, B.K., 1994. Substrate-and nutrient-limited toluene biotransformation in sandy soil. Environmental Toxicology and Chemistry, 13: 693-705.

Allen-King, R.M., Gillham, R.W., Barker, J.F. and Sudicky, E.A., 1996. Fate of dissolved toluene during steady infiltration through unsaturated soil: II. Biotransformation under nutrient-limited conditions. Journal of Environmental Quality, 25: 287-295.

Almeida, J.S., Reis, M.A.M. and Carrondo, M.J.T., 1995. Competition between nitrate and nitrite reduction in denitrification by *Pseudomonas fluorescens*. Biotechnology and Bioengineering, 46: 476-484.

Baedecker, M.J., Cozzarelli, I.M., Siegel, D.I., Bennett, P.C. and Eganhouse, R.P., 1993. Crude oil in a shallow sand and gravel aquifer - III. Biogeochemical reactions and mass balance modeling in anoxic ground water. Applied Geochemistry, 8: 569-586.

Barbieri, M., Carrera, J., Sànchez-Vila, X., Ayora, C., Cama, J., Köck-Schulmeyer, M., Lopez de Alda, M., Barcelo, D., Brunet, J.T. and Garcia, M.H., 2011. Microcosm experiments to control anaerobic redox conditions when studying the fate of organic micropollutants in aquifer material. Journal of Contaminant Hydrology, 126: 330-345.

Beauvais, A., Melfi, A., Nahon, D. and Trescases, J.J., 1987. Pétrologie du gisement latéritique manganésifère d'Azul (Brésil). Mineralium Deposita, 22: 124-134.

Bekins, B.A., Hostettler, W.N., Herkelrath, W.N., Delin, G.N., Warren, E. and Essaid, H.I., 2005. Progression of methanogenic degradation of crude oil in the subsurface. Environmental Geosciences, 12: 139-152.

Bennett, P.C., Hiebert, F.K. and Roberts Rogers, J., 2000. Microbial control of mineral-groundwater equilibria: macroscale to microscale. Hydrogeology Journal, 8: 47-62.

Bregnard, T.P.A., Höhener, P., Häner, A. and Zeyer, J., 1996. Degradation of weathered diesel fuel by microorganisms from a contaminated aquifer in aerobic and anaerobic microcosms. Environmental Toxicology and Chemistry, 15: 299-307.

Brown, C.J., Schoonen, M.A.A. and Candela, J.L., 2000. Geochemical modeling of iron, sulfur, oxygen and carbon in a coastal plain aquifer. Journal of Hydrology, 237: 147-168.

Chakraborty, R. and Coates, J.D., 2005. Hydroxylation and Carboxylation - Two crucial steps of anaerobic benzene degradation by Dechloromonas Strain RCB. Applied and Environmental Microbiology, 71: 5427-5432.

Chapelle, F.H., Bradley, P.M., Thomas, M.A. and McMahon, P.B., 2009. Distinguishing iron-reducing from sulfate-reducing conditions. Ground Water, 47: 300-305.

Coates, J.D., Chakraborty, R. and McInerney, M.J., 2002. Anaerobic benzene biodegradation - a new area. Research in Microbiology, 153: 621-628.

Cozzarelli, I.M., Bekins, B.A., Baedecker, M.J., Aiken, G.R., Eganhouse, R.P. and Tuccillo, M.E., 2001. Progression of natural attenuation processes at a crude-oil spill site - I. Geochemical evolution of the plume. Journal of Contaminant Hydrology, 53: 369-385.

Dibble, J.T. and Bartha, R., 1979. Effect of environmental parameters on the biodegradation of oil sludge. Applied and Environmental Microbiology, 37: 729-739.

Essaid, H.I., Bekins, B.A., Godsy, E.M., Warren, M.J., Baedecker, M.J. and Cozzarelli, I.M., 1995. Simulation of aerobic and anaerobic biodegradation processes at a crude oil spill site. Water Resources Research, 31: 3309-3327.

Essaid, H.I., Bekins, B.A., Herkelrath, W.N. and Delin, G.N., 2011. Crude oil at the Bemidji site: 25 years of monitoring, modeling and understanding. Ground Water, 49: 706-726.

Glass, C. and Silverstein, J., 1998. Denitrification kinetics of high nitrate concentration water: pH effect on inhibition and nitrite accumulation. Water Research, 32: 831-839.

Gran, G., 1950. Determination of the equivalence point in potentiometric titrages. Acta Chemica Scandinavica, 4: 559-577.

Häner, A., Höhener, P. and Zeyer, J., 1997. Degradation of trimethylbenzene isomers by an enrichment culture under N2O-reducing conditions. Applied and Environmental Microbiology, 63: 1171-1174.

Heron, G., Crouzet, C., Bourg, A.C.M. and Christensen, T.H., 1994. Speciation of Fe(II) and Fe(III) in contaminated aquifer sediments using chemical extraction techniques. Environmental Science & Technology, 28: 1698-1705.

Hiebert, F.K. and Bennett, P.C., 1992. Microbial control of silicate weathering in organic-rich ground water. Science, 258: 278-281.

Jakobsen, R. and Postma, D., 1999. Redox zoning, rates of sulfate reduction and interactions with Fe-reduction and methanogenesis in a shallow sandy aquifer, Rømø, Denmark. Geochimica et Cosmochimica Acta, 63: 137-151.

Meckenstock, R.U. and Mouttaki, H., 2011. Anaerobic degradation of non-substituted aromatic hydrocarbons. Current Opinion in Biotechnology, 22: 406-414.

Mills, S.A. and Frankenberger, W.T.J., 1994. Evaluation of phosphorus sources promoting bioremediation of diesel fuel in soil. Bulletin of Environmental Contamination and Toxicology, 53: 280-284.

Naudet, V., Revil, A., Rizzo, E., Bottero, J.-Y. and Bégassat, P., 2004. Groundwater redox conditions and conductivity in a contaminant plume from geoelectrical investigations. Hydrology & Earth System Sciences, 8: 8-22.

Pan, H. and Darvell, B., 2010. Effect of carbonate on hydroxyapatite solubility. Crystal Growth and Design, 10: 845-850.

Parkhurst, D.L. and Appelo, C.A.J., 1999. User's guide to PHREEQC (version 2) - A computer program for speciation, batch-reaction, one-dimensional transport, and inverse geochemical calculations, U. S. Geological Survey, Denver.

Rogers, J.R. and Bennett, P.C., 2004. Mineral stimulation of subsurface microorganisms: release of limiting nutrients from silicates. Chemical Geology, 203: 91-108.

Ryan, J.N. and Gschwend, P.M., 1991. Extraction of iron oxides from sediments using reductive dissolution by Titanium(III). Clays and Clay Minerals, 39: 509-518.

Townsend, G.T., Prince, R.C. and Suflita, J.M., 2003. Anaerobic oxidation of crude oil hydrocarbons by the resident microorganisms of a contaminated anoxic aquifer. Environmental Science & Technology, 37: 5213-5218.

Tuccillo, M.E., Cozzarelli, I.M. and Herman, J.S., 1999. Iron reduction in the sediments of a hydrocarbon-contaminated aquifer. Applied Geochemistry, 14: 655-667.

Ulrich, A.C., Beller, H.R. and Edwards, E.A., 2005. Metabolites detected during biodegradation of 13C6-benzene in nitrate-reducing and methanogenic enrichment cultures. Environmental Science and Technology, 39: 6681-6691.

Viollier, E., Inglett, P.W., Hunter, K., Roychoudhury, A.N. and Van Cappellen, P., 2000. The ferrozine method revisited: Fe(II)/Fe(III) determination in natural waters. Applied Geochemistry, 15: 785-790.

Vogt, C., Kleinsteuber, S. and Richnow, H.H., 2011. Anaerobic benzene degradation by bacteria. Microbial Biotechnology, 4: 710-724.

Weelink, S.A., van Eekert, M.H. and Stams, A.J., 2010. Degradation of BTEX by anaerobic bacteria: physiology and application. Reviews in Environmental Science and Bio/Technology, 9: 359-385.

Table 1. Specifications of every set of microcosms. P in brackets designates sets which were run with addition of 10 mg/L of phosphate.

Microcosms	Name	Water			Headspace	Electron acceptors added	
		From well	Flushed by N_2	Quantity (mL)		Type	Quantity
Sterile	STE	Pz 39	No	102	Air	-	-
Natural	NAT	Pz 39	No	102	Air	-	-
Without oil	OIL-	Pz 39	No	102	Air	-	-
Oxygen	OXY(P)	Pz 39	No	91	Air	Atmospheric oxygen	20.9 %
Nitrate	NIT(P)	Pz 39	Yes	102	N_2	Nitrate solution	150 mg/L
Manganese	MAN(P)	Pz 39	Yes	102	N_2	Cryptomelane	1 g
Iron	FER(P)	Pz 39	Yes	102	N_2	Limonite	1 g
Sulfate	SUL(P)	Pz 23	Yes	102	N_2	Sulfate solution	150 mg/L
Methane	MET(P)	Pz 23	Yes	102	N_2	-	-

Table 2. Depletion of BTEX at the end of the monitoring (series 2). Evaluation was made in % of depletion by comparison to STE microcosms. Negative values indicate that final concentrations were higher than initials. Detection limit was 1 µg/L for benzene (GC-MS), 1.9 µg/L for toluene, ethylbenzene and m+p-xylene (GC-FID), 1.7 µg/L for o-xylene (GC-FID) and 2.1 µg/L for 1,2,4-TMB (GC-FID).

	Benzene	Toluene	Ethylbenzene	*m+p*-xylene	*o*-xylene	*1,2,4*-TMB
NAT	64	-176	88	94	91	57
OXY	100	100	100	100	100	100
NIT	100	-15	100	100	88	100
MAN	68	-95	100	97	95	50
FER	92	-667	100	95	95	45
SUL	100	100	100	100	100	76
MET	85	100	80	86	72	44

Table 3. Results of 0.5 M HCl extractions performed on initial sediments, limonite or cryptomelane. Unit is mg/g air dried mineral.

* Gain represents the additional quantity of Fe(III), Mn or P supplied by limonite or cryptomelane (in % of initial sediment)

	Fe(III)	Mn	P
Sediments	0.48	0.34	0.11
Sediments + limonite (FER(P))	0.51	0.36	0.10
Sediments + cryptomelane (MAN(P))	0.71	1.02	0.10
Gain in initial FER(P) sets *	+6.3 %	+5.9 %	-9.1 %
Gain in initial MAN(P) sets *	+47.9 %	+300 %	-9.1 %

Table 4. Summary of highest rates, type of kinetics and lag phase for each set of microcosms.

* highest rate in NAT has been measured during oxygen consumption

**S-Shaped curve; Monod parameters were not calculated due to a lack of data, especially on biomass concentration

- Type of kinetics not assessable

	highest rate (mmol electron L^{-1} day^{-1})	type of kinetics	lag phase (day)
NAT	1.776*	Monod- with –growth (nitrate and sulfate) first-order (oxygen; half-life time: 6.57 days)	0 (oxygen) 7 (nitrate) 50 (sulfate) 200 (methane)
OXY	0.338	first-order (half-life time: 34.8 days)	0
OXYP	4.499	first-order (half-life time: 2.92 days)	0
NIT	0.108	Monod-with-growth **	14
NITP	0.512	Monod-with-growth **	7
MAN	0.011	-	14
MANP	0.013	-	14
FER	0.0012	-	7
FERP	0.0011	-	7
SUL	0.108	Monod-with-growth **	83
SULP	0.102	Monod-with-growth **	62
MET	0.007	Monod-with-growth **	135
METP	0.036	Monod-with-growth **	78

Fig. 1. Results of STE (A)and OIL-(B) sets. Concentrations in oxygen (♦) and carbon dioxide (□) in sterile microcosms (A), concentrations in nitrate (+) and HCO_3^- (▲) in microcosms without petroleum (B). In line plot, error bars represent standard deviation of measurements in three replicates.

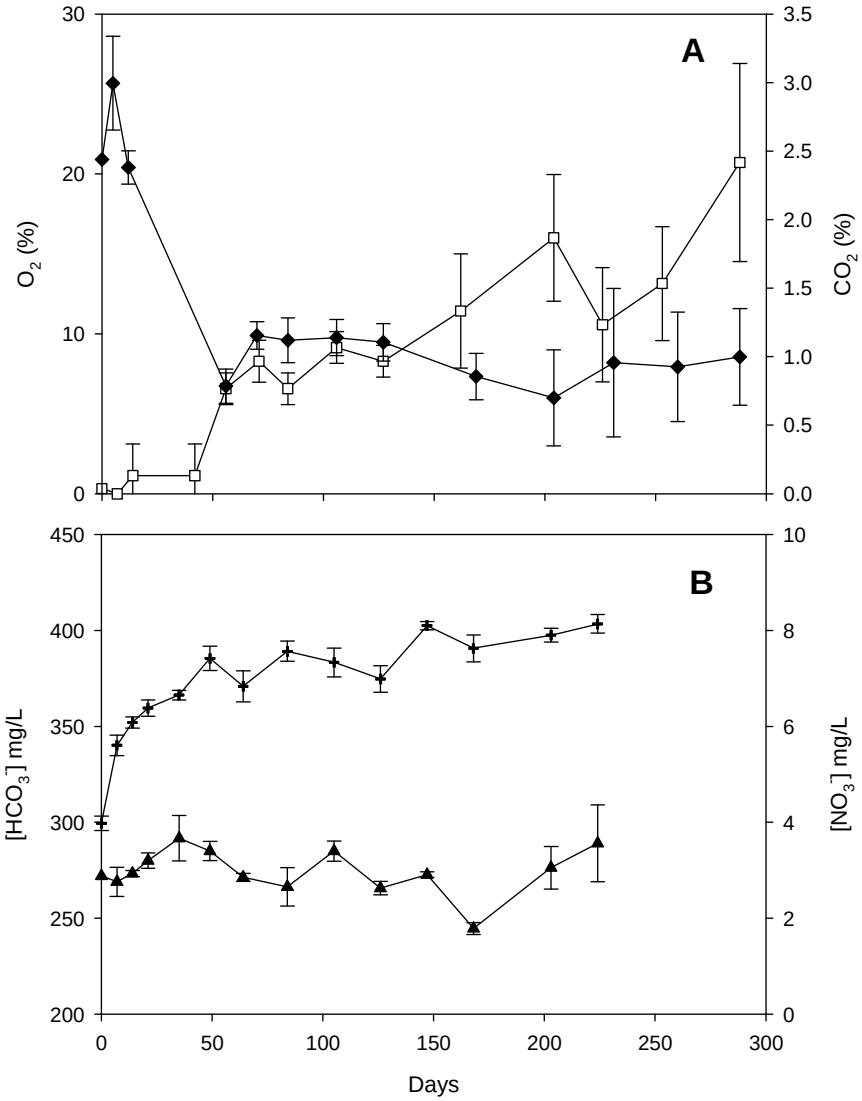

Fig. 2. Results of NAT set. Consumption of oxygen (◊), nitrate (+), sulfate (○), production of methane (■) (A), production of HCO_3^- (▲) and carbon dioxide (□) (B). In scatter plot, one dot represents one analysis in one replicate of the set. In line plot, error bars represent standard deviation of measurements in three replicates.

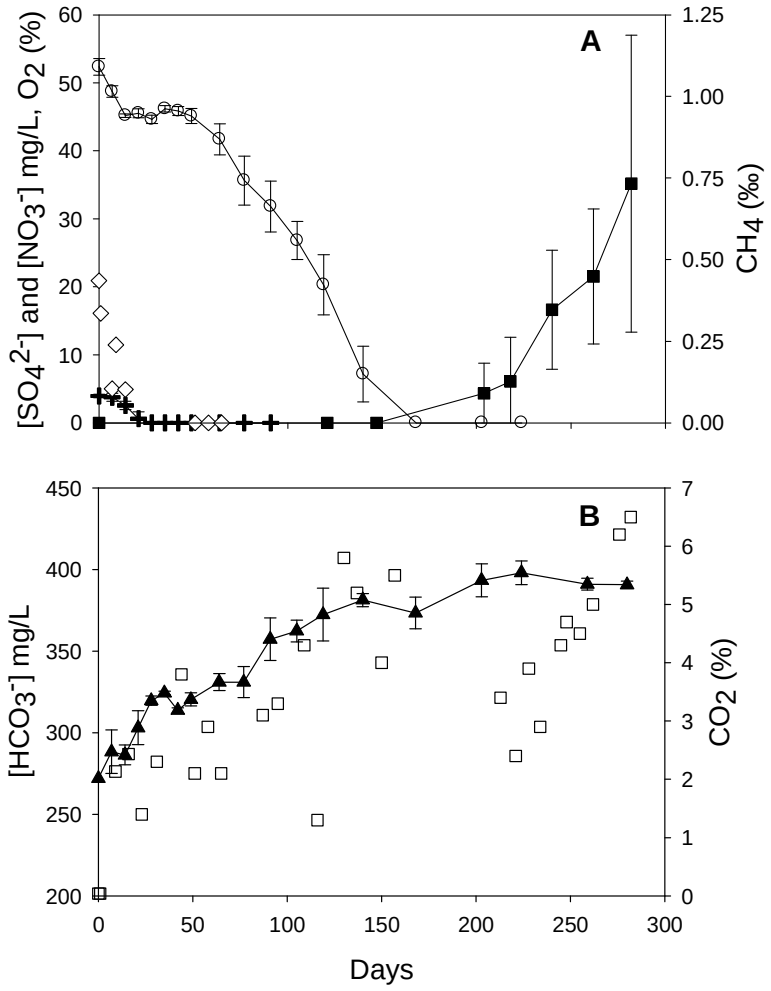

Fig. 3. Results of oxygen and nitrate experiments. Left column: consumption of oxygen (A), production of HCO_3^- (C) and production of carbon dioxide (E) in microcosms OXY (♦) and OXYP (□). Right column: consumption of nitrate (B), production of HCO_3^- (D) and production of carbon dioxide (F) in microcosms NIT (♦) and NITP (□). In scatter plot, one dot represents one analysis in one replicate of the set. In line plot, error bars represent standard deviation of measurements in three replicates. Arrows represent additions of electron acceptors in microcosms of the same set.

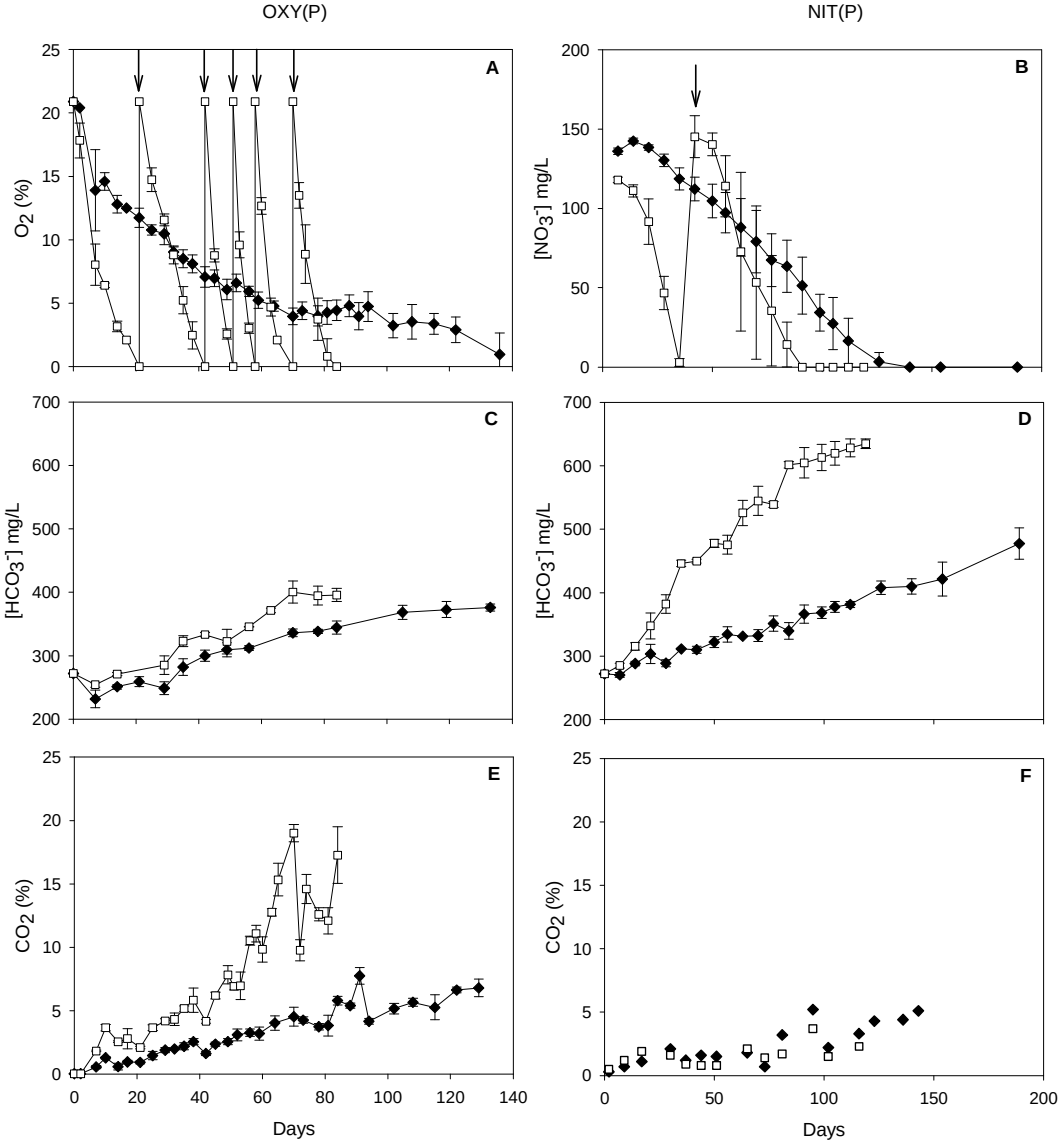

Fig. 4. Results of iron and manganese experiments. Left column: production of dissolved manganese (A), production of HCO_3^- (C) and production of carbon dioxide (E) in microcosms MAN (♦) and MANP (□). Right column: production of dissolved iron (B), production of HCO_3^- (D) and production of carbon dioxide (F) in microcosms FER (♦) and FERP (□). In scatter plot, one dot represents one analysis in one replicate of the set. In line plot, error bars represent standard deviation of measurements in three replicates.

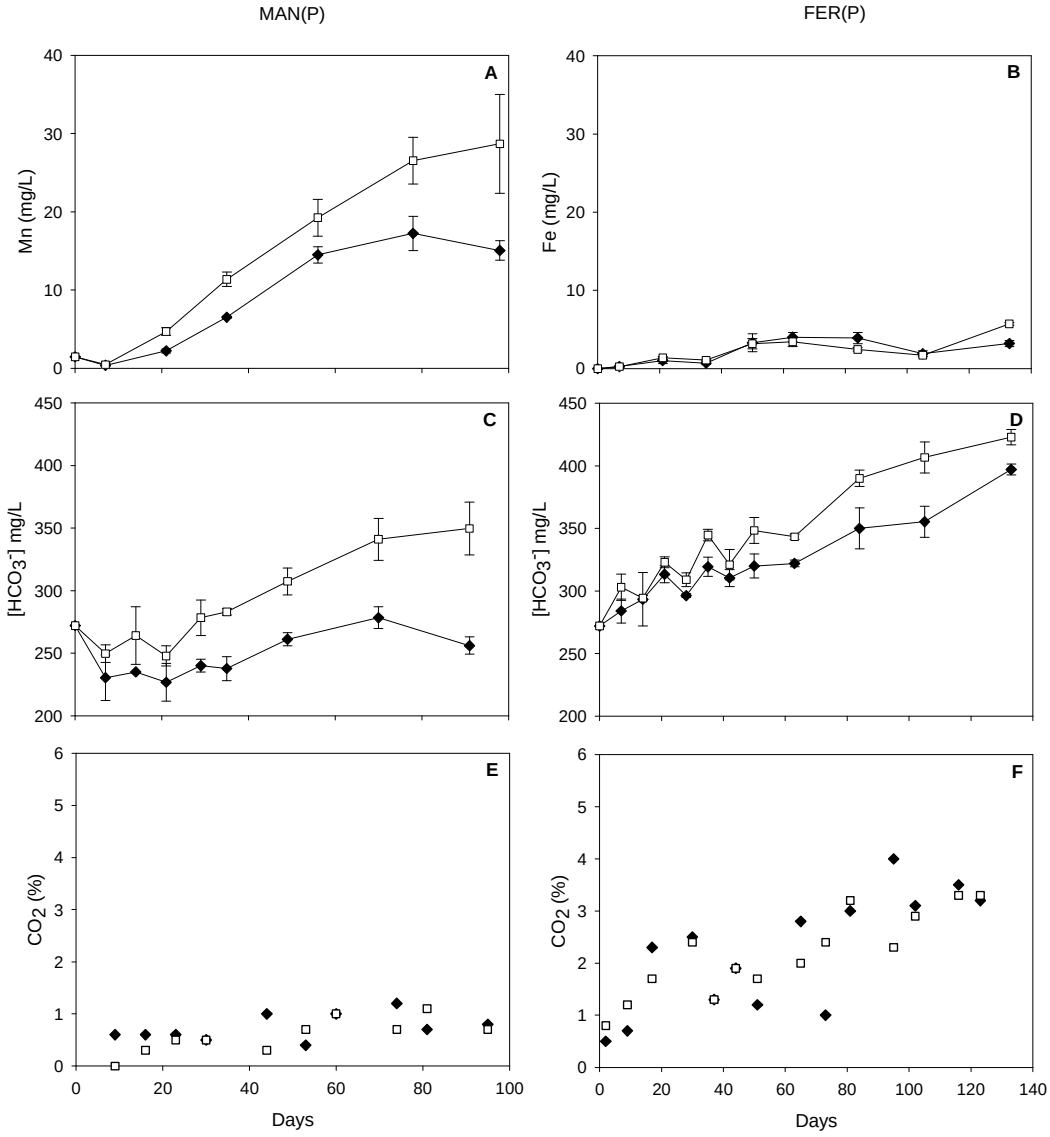

Fig. 5. Results of sulfate and methane experiments. Left column: consumption of sulfate (A), production of HCO_3^- (C) and production of carbon dioxide (E) in microcosms SUL (♦) and SULP (□). Right column: production of methane (B), production of HCO_3^- (D) and production of carbon dioxide (F) in microcosms MET (♦) and METP (□). In scatter plot, one dot represents one analysis in one replicate of the set. In line plot, error bars represent standard deviation of measurements in three replicates.

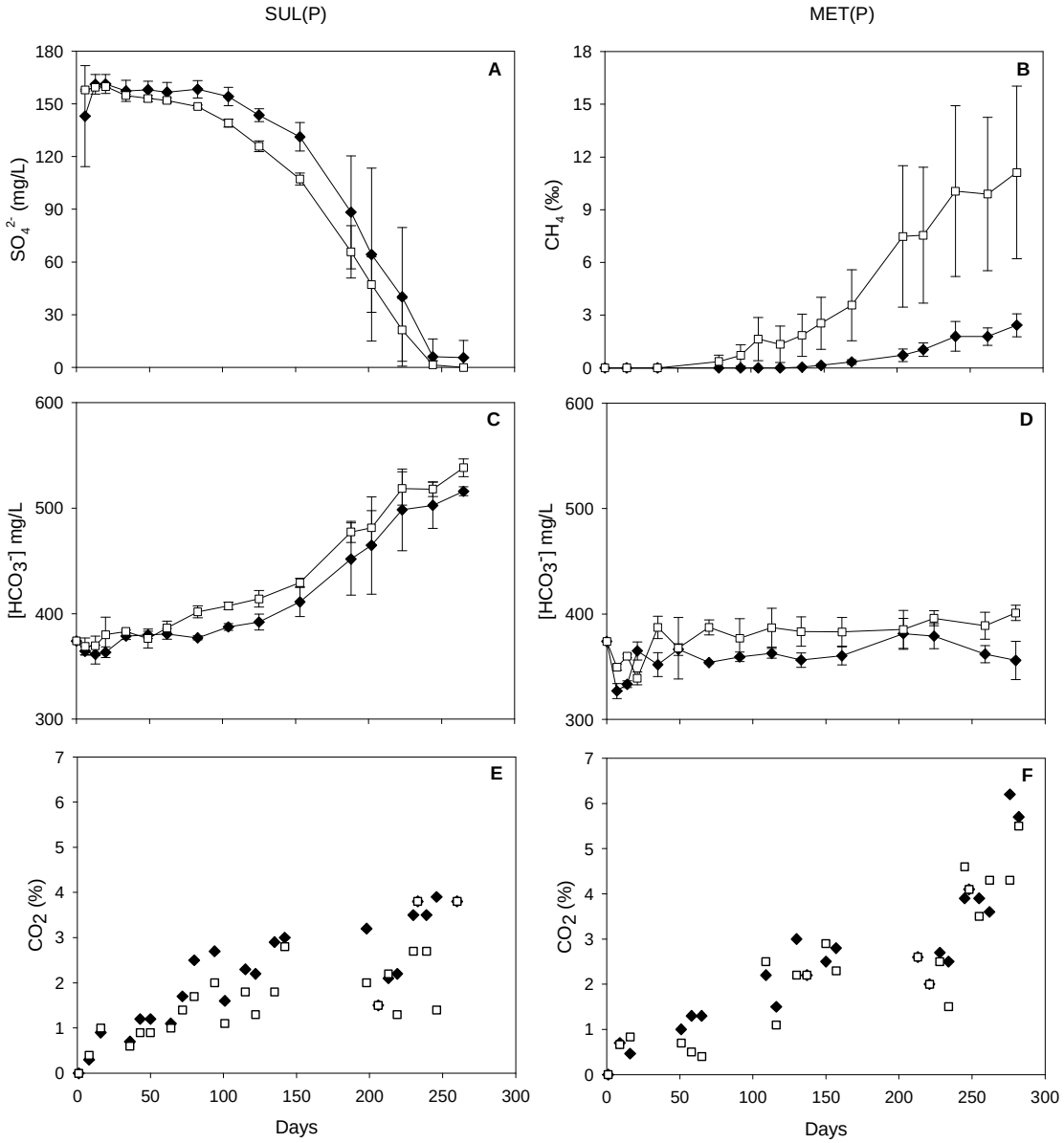

Fig. 6. GC-FID chromatograms of headspace in STE microcosm after 40 days of incubation (=control, A), NIT microcosm after 199 days of incubation (B), and MET microcosm after 312 days of incubation (C). 1, *n*-pentane; 2, *n*-hexane; 3, benzene + cyclohexane; 4, *n*-heptane; 5, toluene; 6, *n*-octane; 7, ethylbenzene; 8, (*m*,*p*)-xylenes; 9, *n*-nonane; 10, *o*-xylene; 11, *n*-decane; 12, *1*,*2*,*4*-TMB; 13, *n*-undecane; 14, *n*-dodecane. Dotted lines represent the same intensity of signal. FID, flame ionization.

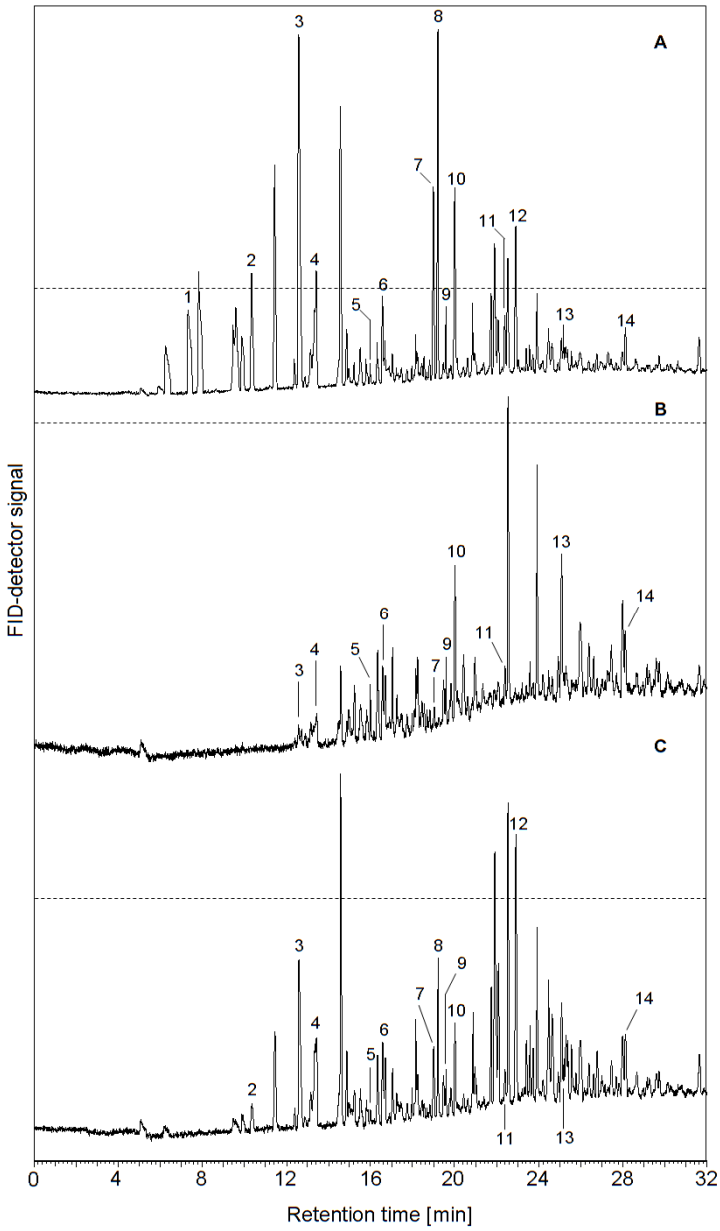

Fig. 7. Temporal evolution of phosphate concentrations in OXYP (A), NITP (B), MANP (C), FERP (D), SULP (E) and METP (F) sets. Arrows represent additions of phosphate in microcosms of the same set, error bars represent standard deviation of measurements in three replicates. (●) show the intermediate time chosen for PHREEQC simulations of saturation index of phosphate-bearing minerals (supp. material).

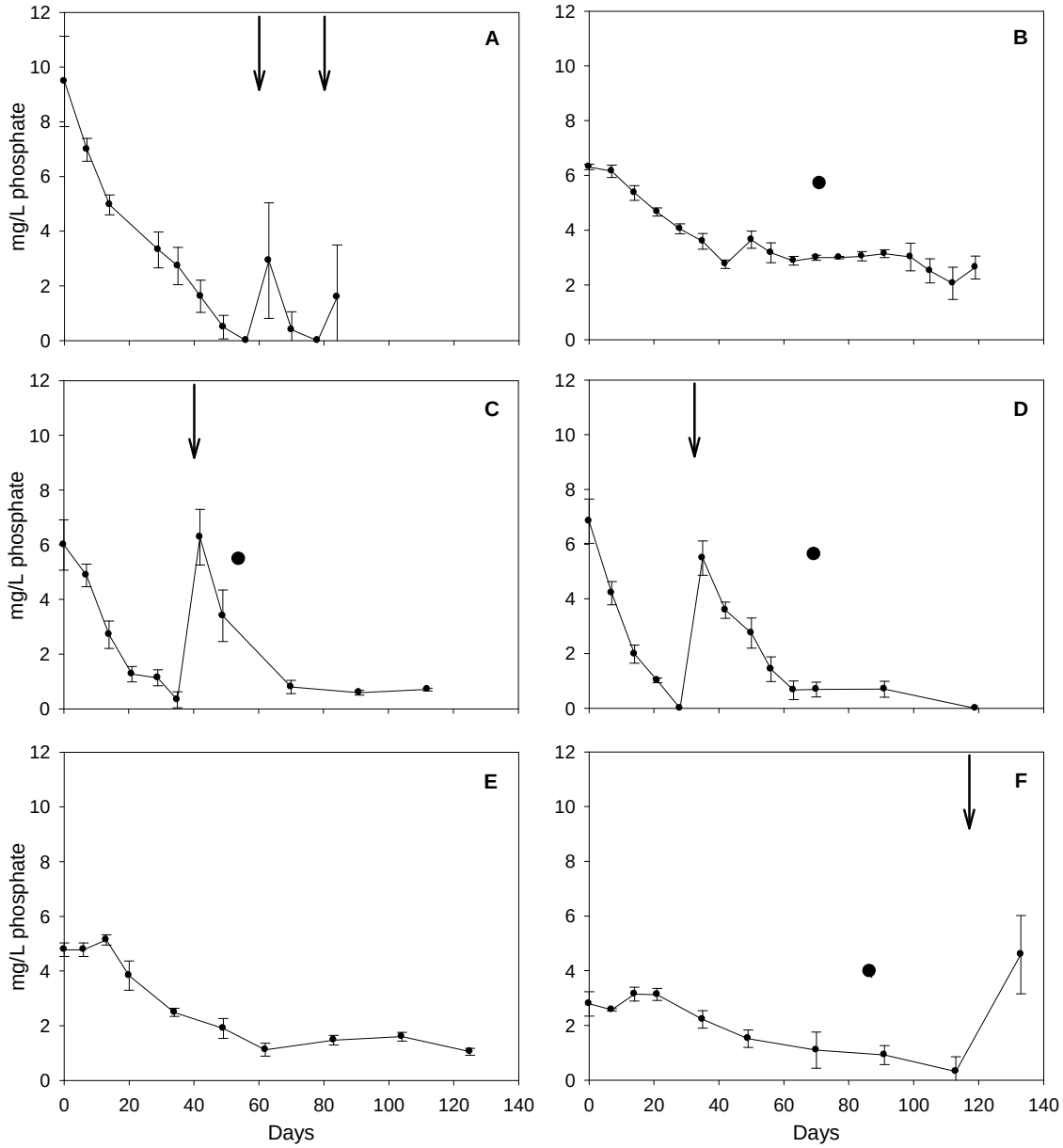

Fig. 8. (A) Mean values of consumption kinetics of electrons acceptors for each series. For MAN(P) and MET(P) series bars stand for production of dissolved manganese and methane respectively. Grey bars for FER(P) sets stands for HCL-extractible precipitated Fe(II) and black bars for dissolved iron. (B) Inorganic carbon produced for each sets (sum of dissolved IC and gaseous CO_2), corrected for sampling losses. Grey bars stand for C-CO_2 produced, black bars for dissolved IC produced. Error bars represent standard deviation of values in three replicates. In both graphs the black line represents the value for NAT microcosms.

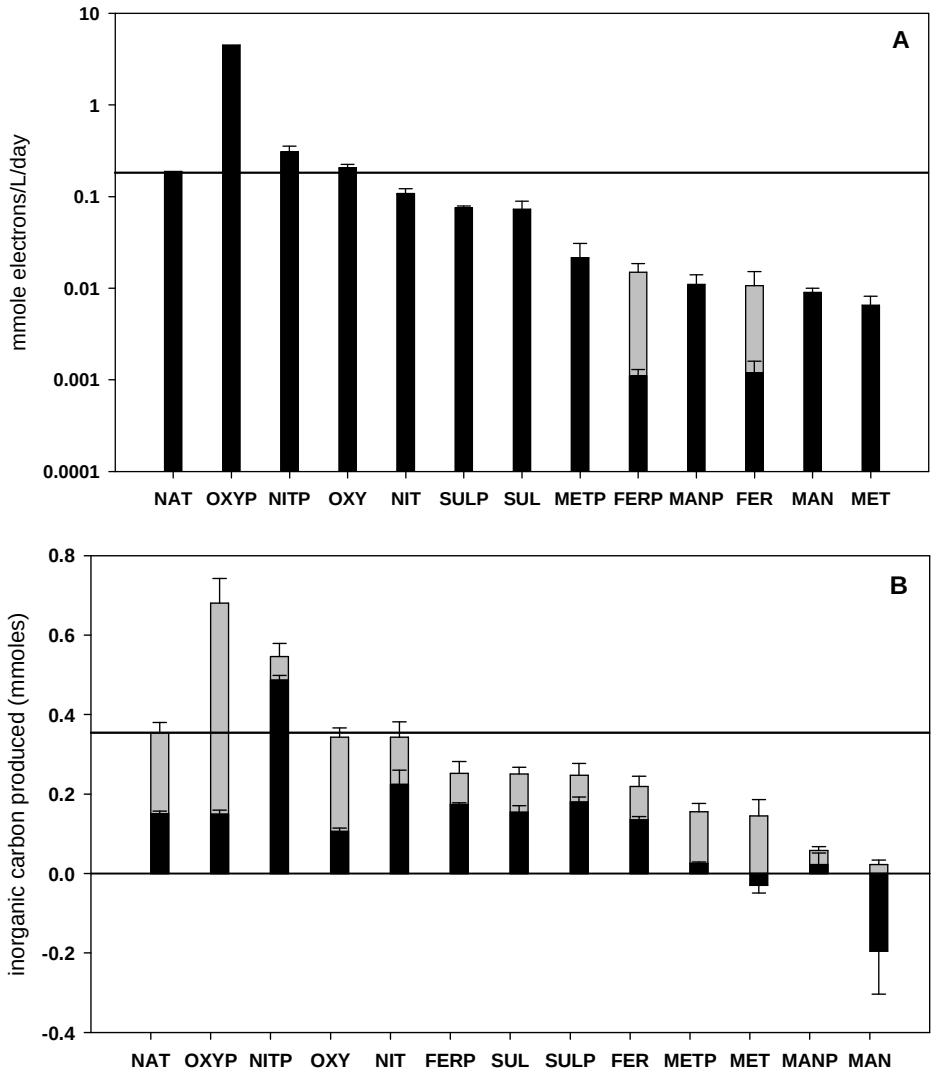

Fig. 9. Saturation Index (SI) of calcite (A), siderite (B) and rhodochrosite (C) at the beginning (light grey) and the end of the monitoring (dark grey) for NAT, MAN(P), FER(P), SUL(P) and MET(P). Error bars represent standard deviation of values in three replicates. SI were modeled with PHREEQC (phreeqc.dat and minteqv4.dat databases).

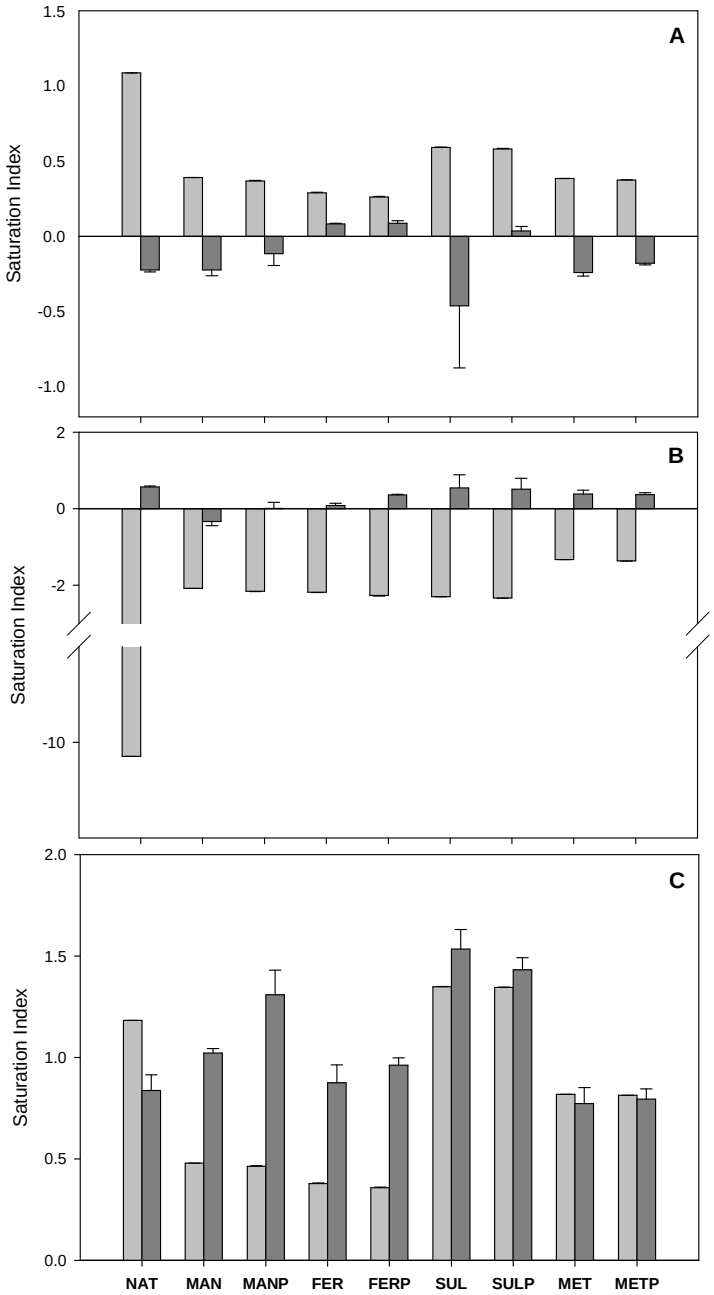

CONHYD 3717: Ponsin et al.

Highlights

- Various redox conditions including methanogenesis were promoted & sustained in microcosms
- Stimulating effect of phosphate on electron acceptors consumption was observed
- Strongest stimulating effect of phosphate was observed in nitrate & oxygen-amended microcosms
- Metal-reducing conditions were limited by availability of electron acceptors
- P decreased lag phase of methanogenesis and stimulated methane production